Controls on gas hydrate system evolution in a region of active fluid flow in the SW Barents Sea

Sunil Vadakkepuliyambatta[1*], Matthew J. Hornbach[2], Stefan Bünz[1], Benjamin J. Phrampus[2]

1 CAGE-Centre for Arctic Gas Hydrate, Environment and Climate, Department of Geology, UiT – The Arctic University of Norway, PO Box 6050 Langnes, N-9037 Tromsø, Norway.

2 Huffington Department of Earth Sciences, Southern Methodist University, PO Box 750395, Dallas, Texas 75275, USA.

*Corresponding author:

Sunil Vadakkepuliyambatta

Department of Geology

UiT- The Arctic University of Norway

Postbox 6050 Langnes

N-9037 Tromsø

Norway.

Phone: +47-77623290

sunil.vadakkepuliyambatta@uit.no

Abstract

The location and stability of gas hydrates in the SW Barents Sea is poorly constrained due to complex geological, geochemical, and geophysical conditions, including poor controls on regional heat flow and gas chemistry. Understanding the stability of gas hydrates in this region is important, as recent studies suggest destabilizing hydrates may lead to methane discharge into the ocean and possibly in to the atmosphere. Here, we use high-resolution 3D P-Cable seismic data, combined with 3D heat flow and fluid flow models to place new constraints on gas hydrate stability in this region. The 3D P-Cable seismic data, acquired in 2009 west of Loppa High, show cross-cutting, reverse polarity, high-amplitude reflectors interpreted as the base of gas hydrate stability. To constrain heat flow, fluid flow, and gas hydrate stability within the 3D seismic volume, we use a 3D steady-state, finite difference diffusive thermal model that incorporates regional bottom water temperature from CTD casts, expected geothermal gradients, and gas composition derived from well data. In general, modelled bottom simulating reflectors are deeper than observed BSRs. Our analysis weighs multiple factors that might explain the discrepancy between observed and modelled bottom simulating reflector depths. From this analysis, we propose that the most significant discrepancies in BSR depth are likely related to changes in regional fluid/heat flow and fluid geochemistry. The anomalously shallow bottom simulating reflectors can be explained via vertical fluid flow that might include ensuing potential effects on gas composition, pore water salinity and temperature. Our estimate suggest that a maximum vertical fluid flux of approximately 12 mm/y is necessary to explain the most significant anomalies. Our study provides new insight into regional heat flow, geochemistry, and end-member vertical fluid flux rates in the Barents Sea. Moreover, it documents that the fluid flow system is active and most likely, very dynamic.

Key words: gas hydrates, fluid flow, BSR, heat flow, Barents Sea

1. Introduction

The Barents Sea is a shallow shelf sea bordering the Arctic Ocean north of continental Europe (Figure 1). It contains large sedimentary basins hosting large amount of hydrocarbon trapped in conventional petroleum systems and innumerable shallow gas and gas hydrate accumulations (Andreassen et al., 1990; Henriksen et al., 2011; Chand et al., 2012; Vadakkepuliyambatta et al., 2013). Submarine natural gas deposits in the SW Barents Sea represent both a potential future energy resource and an environmental risk. Accumulations of free gas and gas hydrate in the shallow subsurface are considered a geohazard (e.g., McIver, 1982; Bugge et al., 1987; Yakushev and Collett, 1992; Driscoll et al., 2000; Mienert et al., 2001). They constitute a risk for safe drilling operations (e.g., Prince, 1990; Grace, 1994; Milkov, 2000; Hovland and Gudmestad, 2001; Ruppel et al., 2008; McConnell et al., 2012) and they may pose a threat to global climate or ocean acidification if they escape from their subseabed reservoir (e.g., Nisbet, 1989; MacDonald, 1990; Nisbet, 2002; Biastoch et al., 2011; Hunter et al., 2013). However, larger accumulations may have economic value and thus, might represent a future natural gas resource (e.g., Peon field, North Sea) as well as provide insight into deeper hydrocarbon accumulations (e.g., Heggland, 1998). Often, shallow gas accumulations result from subsurface fluid seepage from deeper sources (e.g., Hovland and Judd, 1988; Heggland, 1998; Vadakkepuliyambatta et al., 2013), and these shallow accumulations sometimes form gas hydrates when suitable conditions exist (e.g., Shipley et al., 1979; Clennell et al., 1999; Kvenvolden and Lorenson, 2001; Andreassen et al., 2007). The depth at which hydrates form depend directly on the gas geochemistry (Sloan and Koh, 2008), and therefore, the formation depth of gas hydrates provide

indirect insight into thermogenic hydrocarbon sources. Gas hydrate, an ice-like substrate, consists mainly of light hydrocarbons (mostly methane) entrapped by a rigid cage of water molecules (Sloan and Koh, 2008). Gas hydrates may contain more carbon than all other global hydrocarbon reservoirs, but the size of the gas hydrate reservoir as well as the free gas reservoir usually trapped just below the hydrate stability zone remains highly debated (e.g., Dobrynin et al., 1981; Kvenvolden, 1988; Holbrook et al., 1996; Dickens et al., 1997; Milkov et al., 2003; Hornbach et al., 2012). Thus, developing better techniques for detecting, quantifying, and understanding the occurrence of gas hydrate, particularly in the SW Barents Sea, where significant hydrocarbon provinces exist, remains an important challenge.

The Barents Sea represents an important region for gas hydrate research because (1) of its shallow depth and its inherent sensitivity to future ocean warming, (2) its widespread fluid expulsion system (Chand et al., 2012; Vadakkepuliyambatta et al., 2013), and (3) the area is a major oil and gas exploration region, where hydrates represent a potentially significant drilling hazard. Here, we conduct a detailed 3D analysis of gas hydrate stability above a major fluid-flow structure in the vicinity of the Polheim Sub-Platform in the SW Barents Sea in a water depth of ~300 m, where gas hydrate can exist. Specifically, we use high-resolution P-Cable 3D seismic data to construct a 3D steady-state heat flow model to constrain the region of hydrate stability. This method has been successfully applied at other sites to estimate not only regional heat flow but locate regions of elevated fluid flow and elevated hydrate concentrations (Hornbach et al., 2012). For this analysis, we compare model results to observations of Bottom Simulating Reflectors (BSRs) in seismic data representing the base of hydrate stability in submarine sediments. We use differences between model predictions and observations to further improve our understanding of where hydrate is stable in the Barents Sea, and what governs stability

conditions. Our analysis places end-member estimates on fluid advection rates towards shallow sediments and therefore offers new insight into not only regional heat flow and geochemistry, but also fluid flux into the hydrate stability zone, and perhaps the oceans, in the SW Barents Sea.

2. Gas Hydrate Stability

Gas hydrate formation in marine sediments requires natural gas and water existing at very specific pressure and temperature (Claypool and Kaplan, 1974; Kvenvolden, 1988; Clennell et al., 1999). The stability of hydrates is affected by the composition of gas and ionic impurities in the water (Kvenvolden, 1998; Sloan and Koh, 2008). These constraints on hydrate formation define the gas hydrate stability zone (GHSZ) —the limited depth/pressure range in which gas hydrates are stable. Anomalous reflections in the seismic data, known as BSRs (Bottom Simulating Reflectors), mark the bottom of the GHSZ and suggest the possible presence of hydrates in marine sediments above (Shipley et al., 1979; Holbrook et al., 1996; Bünz et al., 2003). The BSR has high reflection amplitude and is normally of reverse polarity. This reflection is usually the result of relatively stiff hydrate-bearing layer (high acoustic velocity) overlying gassy sediment (low acoustic velocity). In an environment where the gas composition, water composition, sediment composition, and regional heat flow are relatively homogenous and stable, the BSR mimics the seabed topography and cuts across normal reflections produced by slight changes in density and sonic velocity (e.g., Shipley et al., 1979).

A significant portion of the hydrocarbons in the SW Barents Sea has leaked or migrated into the shallow subsurface and is now trapped in gas-hydrate and shallow-gas reservoirs (e.g., Chand et al., 2012; Vadakkepuliyambatta et al., 2013). Most of the gas is assumed to be leaking from Jurassic formations which encompass significant portion of the proven hydrocarbon resources in

the region (Doré, 1995). Leakage of gas into the shallow sediments was probably a result of the profound Cenozoic erosion of the Barents Sea shelf (Knies et al., 2009; Henriksen et al., 2011). The ultimate timing of the deep leakage remains questionable and whether it occurred periodically over millions of years or abruptly during glacial-interglacial cycles is unclear.

3. Geological setting and gas hydrates in the SW Barents Sea

The SW Barents Sea consists of a mosaic of basins, platforms, and structural highs and has a complex tectonic history (Gudlaugsson et al., 1998). Many studies describe in detail the geologic evolution of the Barents Sea (Gabrielsen et al., 1990; Faleide et al., 1993). The Barents Sea area was affected by extensive uplift and erosion during the Late Cenozoic (Nøttvedt et al., 1988; Vorren et al., 1988; Vorren et al., 1991). Sediment erosion during various glaciation periods has controlled the geomorphology of the SW Barents Sea (Vorren et al., 1991; Riis and Fjeldskaar, 1992), and had a major impact on the petroleum systems of the area (Doré and Jensen, 1996; Henriksen et al., 2011). Geotechnical and geochemical data suggest an erosion of approximately 1000 m in the SW Barents Sea (Nyland et al., 1992). The area was also affected by periods of glaciations and during the late Weichselian glaciation the ice cap thickness exceeded 1500-1700 m (Svendsen et al., 2004), which was followed by late Cenozoic uplift of 900-1400 m, associated with erosion and glaciation(Riis and Fjeldskaar, 1992).

Our detailed study area in the SW Barents Sea is situated on the Polheim Sub-Platform, between the Ringvassøy-Loppa Fault Complex (RLFC) and the Loppa High (Figure 1), a structural high associated with the late Jurassic to early Cretaceous and Tertiary deformational events (Gabrielsen et al., 1990). The RLFC is dominated by normal faulting (Faleide et al., 1984) and is

associated with the large-scale extensional rifting during the mid-Jurassic to early Cretaceous (Talleraas, 1979). Reactivation took place in the late Cretaceous.

Extensional tectonics, glacial erosion and associated uplift have resulted in the spillage of hydrocarbons from filled reservoirs (Kjemperud and Fjeldskaar, 1992; Doré and Jensen, 1996). As a result, surface and subsurface fluid seepage features are present on all parts of the SW Barents Sea (e.g., Andreassen et al., 2007; Chand et al., 2008; Perez-Garcia et al., 2009; Ostanin et al., 2012; Vadakkepuliyambatta et al., 2013). Most of these features show associated shallow gas accumulations and gas hydrates above these reservoirs. Gas hydrates are inferred from interpreted BSRs on many parts of the Barents Sea (e.g., Andreassen et al., 1990; Løvø et al., 1990; Laberg and Andreassen, 1996; Chand et al., 2012). Previous gas hydrate stability modelling show a highly variable GHSZ in the SW Barents Sea region, mainly controlled by higher-order hydrocarbon gases, significant variations in heat flow, changes in thermal conductivity and geochemistry associated with subsurface salt and salt tectonics, and glacial episodes (Chand et al., 2008). Adding to the complexity of gas hydrates occurrence in the SW Barents Sea is that pure methane hydrates are not stable on most parts of the SW Barents Sea, but assuming the presence of higher-order hydrocarbons, the GHSZ could extend as much as 800 m beneath the seafloor (Chand et al., 2008). The locations of apparent BSRs in the seismic data support the existence of thermogenic gases from deeper sources (e.g., Laberg et al., 1998; Chand et al., 2012), and knowing the geochemistry of the gas is an important factor controlling the depth of gas hydrate stability at this site.

A host of geological, geochemical, and geophysical factors control the depth and location of gas hydrate stability, and it is critical to account for each of these factors correctly to make an accurate assessment of the GHSZ (Sloan and Koh, 2008; Hornbach et al., 2012; Phrampus and

Hornbach, 2012). Important parameters affecting hydrate formation include bottom water temperature, geothermal gradient, gas composition, and pore water salinity (Ussler and Paull, 2001; Coffin et al., 2007). Some of these parameters are highly variable in the SW Barents Sea. Different water masses control the bottom water temperatures in the Barents Sea region (Løvø et al., 1990). In general, the northern part of the SW Barents Sea is significantly colder than the southern part due to the influence of cold Arctic water masses, and the bottom water temperature in our study area (320 m) may in some extreme cases vary between -1.5 ^{0}C to 6.5 ^{0}C (NODC, 2013).Seasonal variation in bottom water temperature is relatively small (about 1 ^{0}C) and most prevalent close to the coastline and in the northern part of SW Barents Sea.

Another additional complexity is that unlike the Hydrate Ridge, Cascadia, or Blake Ridge, few heat flow measurements exist in the SW Barents Sea to constrain regional shallow subsurface temperatures. This is compounded by the fact that heat flow in some parts of the SW Barents Sea can be locally variable due to the presence of piercement structures, such as salt domes in the Nordkapp Basin and the Tromsø Basin (Bugge et al., 2002). Salt intrusions typically increase both shallow sediment temperatures and pore water salinity, resulting in a thinner GHSZ (e.g., Dickens and Quinby-Hunt, 1997; Taylor et al., 2000; Hornbach et al., 2005; Ruppel, 2005; Sloan and Koh, 2008). Faults and focused fluid flow features can also increase heat flow causing a shallower GHSZ (e.g., Ruppel, 2005). The major source of information on geothermal gradients in the SW Barents Sea is bottom-hole temperature measurements from deep exploration wells. Existing geothermal gradient measurements from wells show significant regional variability. For example, in the Nordkapp Basin, the geothermal gradient varies from 22.8-69 ^{0}C/km within relatively short distances (~120km) (Bugge et al., 2002) and this variation can shift the GHSZ ~300 m vertically over a broad region at this site (Chand et al., 2008).

Gas composition in sediments in the SW Barents Sea is also highly variable. Knowledge of precise gas composition is important in gas hydrate stability modelling, as even a moderate (5-10%) variation in gas composition can shift the modelled GHSZ by tens-to-hundreds of meters (Chand et al., 2008; Sloan and Koh, 2008; Collett et al., 2009). Chemical analyses of gas samples in the water column and beneath the seabed along the Svalbard Barents Sea margin indicate a complex thermogenic origin (Løberg and Bjorøy, 1990; Knies et al., 2004). Middle-lower Jurassic sandstones are the primary reservoirs in the SW Barents Sea (Larsen et al., 1993), and gas expansion (Nyland et al., 1992) and reservoir tilting (Kjemperud and Fjeldskaar, 1992) has likely resulted in leakage of higher-order (i.e. non-methane) hydrocarbons from deeper formations in the Bjørnøya Basin and the Hammerfest Basin (Larsen et al., 1993). Considering these factors, Laberg and Andreassen (1996) suggested a thermogenic origin implying higher-order hydrocarbons likely exist in gas hydrates observed in the Bjørnøya Basin. Analyses conducted on gas samples from deep exploration wells in the SW Barents Sea show presence of higher-order hydrocarbons, as high as 30% (NPD). As a result, we can use the depth of the seismic BSR to place constraints on (1) the geochemical signature of the gas and (2) from this, the potential source depth of thermogenic gas migration below the Barents Sea 3D volume.

We therefore use our model to estimate possible BSR locations in the area using end-member values for different geochemical and geophysical parameters, and from this, derive first-order estimates for the potential controls on hydrate stability at this site.

4. Seismic data collection and interpretation

We acquired high resolution P-Cable (Planke et al., 2009) 3D seismic data in 2009 using twelve 25 m long streamers, spaced 15m apart and one GI gun (2x45cc) firing every 5 seconds at a

pressure of approx. 150 bars. Data processing followed the procedure described in Rajan et al. (2013) and consisted of navigational correction, binning, static and tidal correction, band pass filtering, amplitude correction, trace editing, normal move-out, 3D stack and 3D stolt migration. The lateral resolution of the survey is 6.25x6.25 m. In addition to the seismic data, well log data from nearby exploration well 7219/9-1 is used to constrain seismic velocity.

The seafloor in the study area is highly uneven (Figure 2a). Linear depressions, 30 to 200 m wide, crisscross the seafloor surface and are interpreted as glacial ploughmarks. They are the most common features on the seafloor in the SW Barents Sea, resulting from seabed erosion by glaciers (Elverhøi and Solheim, 1983). High-amplitude reflections, showing reverse polarity, are identified in the study area below the Upper Regional Unconformity (URU) (Figure 2a). The URU is a major reflector in the Norwegian Shelf areas, formed during late Pliocene-Pleistocene (Eidvin et al., 1993), which separates glacial sediments from pre-glacial sedimentary rocks. At an arrival time of approximately ~610 ms, we observe discontinuous, high amplitude reflections below the URU. This high amplitude, reversed polarity reflection indicates the presence of gas-rich sediments. Moreover, the reflection cross-cuts sedimentary strata and generally mimics the shape of the seafloor and thus, is interpreted as the base of the GHSZ in this region (figure 2a, b,c). We therefore define this feature as a BSR associated with the gas hydrate phase boundary. This interpretation is consistent with previous studies that have also documented the existence of gas hydrates at this site (Løvø et al., 1990). We generally observe chaotic, discontinuous reflections below the BSR. The top of the BSR is discontinuous, as is documented with an RMS amplitude attribute map, implying potentially significant variability of gas and perhaps gas hydrate concentration across the region (Figure 3a). Specifically, in map view, the BSR assumes isolated, elongated, and oval-shaped patterns from 50 to 1400 m wide.

West-to-east profiles through the 2D seismic data shows the BSR with intermittent vertical zones of heavily attenuated seismic signals below (Figure 3b). Such regions of low amplitude, chaotic or noisy seismic signals are observed in many parts of the SW Barents Sea, and often recognized as indicators of upward migration of fluids (Gorman et al., 2002; Vadakkepuliyambatta et al., 2013). The noisy acoustic signals below the BSR mask much of the subsurface structure beneath, making interpretation for the nature of fluid migration below difficult. At some locations, vertical conduits appear to cut through the surrounding lithology (Figure 3). Termination of high-amplitude gas-rich reflections into vertical fluid conduits and BSRs also supports the hypothesis of upward fluid migration in this region. The consistency between 2D and 3D images at this site (with the 3D properly migrated to improve resolution in all directions and to reveal true-amplitude features) rule out the interpretation of these features as migration artefacts.

_ENREF_45 As discussed previously, we can attribute the irregular and discontinuous nature of the BSR to a host of geochemical and geophysical factors. Additionally, variations in sediment physical properties and gas supply can also effect the existence, location, and pervasiveness of the BSR (Woodside and Ivanov, 2002). However, to form the dipping terminations as seen in figure 2b and 2c, significant local variation in the parameters that control hydrate stability may be necessary.

In order to understand what physical conditions can lead to the formation of such a seismic reflection, we implement a high-resolution 3D steady-state heat flow model using the P-Cable data that integrates gas hydrate stability models to estimate BSR depth (Hornbach et al., 2012).

5. 3D diffusive heat flow model and gas hydrate stability zone modelling

To generate a 3D steady-state thermal model, we use a variation of the 3D finite difference diffusive thermal model adapted from Hornbach et al. (2012) which utilizes 3D seismic data and well data in the study area to constrain the geometry, sediment diffusivity, and geothermal gradient across the region. The lateral resolution of the model is 200x200 m. The vertical resolution of the model is 10m and the total depth of the model is 3000 m. The geothermal gradient in the area is calculated using bottom-hole temperatures from well 7219/9-1. Bottom-hole temperatures are usually inaccurate indicators of temperature with depth if they are not corrected for drilling effects (e.g., Cavanagh et al., 2006), and we therefore apply a standard Horner correction to estimate bottom-hole temperature and its associated uncertainty (e.g., Peters and Nelson, 2009) (Figure 4a). This approach yields a geothermal gradient of $31.3 \pm 3\ ^{0}$C/km (1 sigma), and is consistent with other regional studies (Bugge et al., 2002). There are no reported evidences of salt domes in this area which makes the thermal gradient estimation reliable. The thermal conductivity, density, and specific heat capacity of the sediments are adapted from Duran et al. (2013), and are 2.06 ± 0.89 W/m/K, 2702 ± 21.23 kg/m^3, and 885.75 ± 25.1 J/kg/K respectively. Because the P-Cable seismic system uses short streamers, limited seismic velocity data exists at this site. The check-shot velocity measurements from the well 7219/9-1 are used to convert the modelled BSR to the time domain (Figure 4b). The sediments overlying the BSR are similar at the locations of both well and seismic data, which rules out significant variations in average velocity of sediments.

The diffusive thermal model has Dirichlet boundary conditions, with temperature increasing linearly with depth below the seafloor at side boundaries, and constant temperature at the bottom boundary that assumes a linear increase in temperature with depth. Seafloor temperatures are

held constant over time but vary with water depth consistent with CTD casts from the area (NODC, 2013) (Figure 4c).

Results from the 3D diffusive heat flow model provides a steady state temperature-depth profile across the 3D dataset that accounts for changes in seafloor bathymetry and varying conductivity (Figure 5a). Using the model results, the depth of the BSR is estimated using standard gas hydrate phase boundary methods (e.g., Sloan and Koh, 2008). We assume hydrostatic pressures, pore water salinity of 35‰ and gas composition with 97.04% of methane, 0.96% of ethane, 1.31% of propane, and 0.69% of butane, as observed in the nearby well 7219/9-1.

The model-estimated BSR depth in the area varies between 530-540 m below sea level (Figure 5b). At most locations, the model-predicted BSR is deeper than the interpreted BSR in the 3D data set by more than 40 m.

6. Analysis and Discussion

Subtracting modelled steady-state BSR depths from seismically imaged BSR depth in the area suggests an anomalously shallow BSR across the area based on our assumed parameters (Figure 5c). The largest anomaly between the observed and modelled BSR is about 55 m. The fact that model predictions do not match the observed BSR implies either incorrect model parameters (such as incorrect physical properties assumptions), or non-steady-state conditions exist in the study area. Here, we analyse what potential changes in model assumptions are necessary to explain the discrepancy between model results and observations. Importantly, this work focuses solely on what may cause small-scale (tens of meters) changes to the BSR depth over small areas within the 3D seismic survey (i.e. BSR changes occurring over areas on the order of m^2 to <1 km^2). Sea level changes, uplift and erosion, ocean temperature variations, and glaciations are

known to influence the gas hydrate stability zone (e.g., Chand et al., 2012; Phrampus and Hornbach, 2012) yet these processes typically occur broadly (10s to 100 km^2) across the region, and are therefore ignored here. Seasonal bottom water temperature variations are unlikely to cause variations in the BSR depth situated hundreds of meters below the seafloor as it would take more than 100 years for these seasonal effects to propagate fully to BSR depths. Uncertainties in thermal conductivity and density of the sediments have only a marginal impact on the BSR depth (<10m), indicating other factors play a more significant role in defining the base of GHSZ.

6.1 Uncertainties in the model

6.1.1 Salinity of pore fluid

Increasing the salinity of pore fluid due to localized fluid flow associated with salt diapirs and deeper, more saline formations can inhibit the formation of hydrates, resulting in a shallower BSR than the model predicts (e.g., Chand et al., 2008; Sloan and Koh, 2008). Currently, there is no indication from regional drilling near this site that elevated salinities exist in the pore fluid. Although evaporites do exist in the SW Barents Sea (Gabrielsen et al., 1990), to our knowledge, no evaporites have been identified below or within 50 km of the study area. Formation water in some deep reservoirs have a wide range of salinities (7-270 ‰) owing to water mixing and other physical and chemical processes; the presence of evaporites can also result in high salinity (35-350 ‰) formation water (Warren, 2006; Abdou et al., 2011). Pham et al. (2011) calculated the salinity of Tubåen formation (2600 m deep) in the Snøhvit field located in the Hammerfest Basin (Figure 1) to be 168 ‰.

To determine the role salinity may play in the discrepancy between the interpreted versus modelled base of hydrate stability, we vary salinity in the model, holding all other parameters

constant (Figure 6). Gas hydrates are unstable in the area for the maximum possible salinity of formation water (168 ‰). Even if we use the salinity of the Tubåen formation, the hydrates are found to be unstable in the area. We calculate that to cause the maximum observed shallow anomaly in the BSR depth (assuming no advection), the salinity of the pore fluid should be no greater than 51 ‰. Thus, a near uniform increase of ~55% in the pore water salinity provides one explanation for the anomalously shallow BSR we observe in the seismic data. We hypothesize that upward migration of highly saline fluids must be present in the study area for such changes in salinity since, as noted earlier, there is no indication from regional drilling results of elevated salinity near this site.

6.1.2 Gas composition

Composition of the gas that forms hydrate directly affects the GHSZ (Kvenvolden, 1998; Sloan and Koh, 2008). Biogenic (methane) gas hydrates are more stable at shallower depths below the seafloor than thermogenic gas hydrates that contain higher-order hydrocarbons (Chand et al., 2008). For the hydrate stability model we developed, the reservoir gas composition from well 7219/9-1 is used which contains ~3% of higher-order hydrocarbons. However, gas composition may vary as it migrates upwards through different formations or evolves from different source rock. Comparison of gas composition between well sites indicates that in the most extreme cases, bulk methane composition changes by as much as 32% in the SW Barents Sea sediments (68.1-100%, from well reports, NPD). Pure methane hydrates are unstable in the study area. We estimate the BSR can be as deep as 760 m taking the measured end-member variation in methane concentration across the SW Barents Sea into account (Figure 6). Our calculations suggest a 0.7% increase in methane (such that methane constitutes 97.74% of the gas) could explain the maximum observed BSR depth anomaly (55 m) in the seismic data. We therefore hypothesize

that progressively increasing concentrations of methane (that is molecularly lighter and more buoyant) than other natural gases might also explain the anomalously shallow BSR. Without shallow drilling data at the site, however, it is very difficult to determine accurately whether change in gas composition causes the observed anomaly in BSR depth.

6.1.3 Regional heat flow and associated geothermal gradient

Temperature variations associated with changes in regional heat flow can also affect the stability of gas hydrates (e.g., Sloan and Koh, 2008). For constant thermal conductivities, increases in heat flow will increase the regional geothermal gradient, resulting in shallower BSRs. Using well data, we calculate a geothermal gradient at this site of 31.3 ±8 °C/km (Figure 4a), and from this a regional heat flow of 41 ± 10.4 mW/m^2. This corresponds to a variation in the BSR depth between 450 m and 690 m below sea level (Figure 6). Although, this variation can easily account for the maximum observed anomaly in the BSR depth, if heat flow is truly diffusive in nature, it is unlikely that the error in the geothermal gradient calculation can explain the small (meter-scale) lateral variations in BSR depth observed in this area. However, there may well be local added heat flow associated with vertical fluid flux, as we shall demonstrate later in this paper.

6.1.4 Anomalous seismic velocity due to lithology changes or gas hydrate accumulations

Seismic velocities from well 7219/9-1, located ~15 km away, are used to convert the BSR depth to two-way time. Our calculations estimate that an uncertainty of 10% in the seismic velocity could account for the observed BSR anomaly. However, this still cannot explain the dipping edges of observed BSRs (Fig. 2b, c). Moreover, the seismic data do not show any significant variation in lithology above the BSR so as to cause a velocity anomaly.

Seismic P-wave velocities in pure gas hydrate is more than twice that of typical shallowly buried marine sediments (Waite et al., 2000). High concentrations of hydrates above BSRs can lead to unexpectedly high seismic velocities (e.g., Gorman et al., 2002). If these anomalous velocities are unaccounted for in the seismic velocity model, they can cause unexpected BSR shoaling (Gorman et al., 2002; Hornbach et al., 2003). We calculate the amount of hydrate necessary in the sediment to explain the shift in depth using the rock physics model of Helgerud et al. (1999). For this calculation, we assume sediment above the BSR consists of sandy clay with a maximum average porosity of 45%, an average number of grain contacts of 8.5, a seismic velocity of 1750 m/s without the hydrates. If hydrate cements the sediment frame, the BSR depth anomaly can be explained only if 50% of the entire sediment column above the BSR consists of hydrate. This is highly unlikely since the glacial deposits in the SW Barents Sea are not suitable hydrate reservoirs. A conservative estimate by Laberg et al. (1998) from a nearby area show hydrate occupancies up to 7% of the sediment volume. Thus, it is unlikely that seismic velocity anomalies due to elevated hydrate concentrations explain the observed shoaling of BSR.

6.2 Assessing fluid flow as an alternative explanation for the BSR

From uncertainty analysis already discussed, we can conclude that changes in our assumptions regarding salinity, gas composition and geothermal gradient may act alone or perhaps in concert to produce some of the observed differences between the true and modelled BSR at this site. Although diffusion of gas and salinity across the site is possible, advective flow provides by far the most effective means of changing the regional geochemistry and temperature across the site (e.g., Bredehoeft and Papadopulos, 1965) and also provides at least one explanation for the small (meter) scale lateral changes we observe in BSR depth in the seismic volume. Here, we assess

how fluid flow might provide an alternative explanation for the difference between the modelled and observed BSR.

The seismic data show a large zone of acoustic masking below the observed BSR, indicating attenuation of wave energy or possible disorganized and chaotic seismic reflections below (Figure 2, 3). Such acoustically masked zones are often interpreted as gas chimneys, formed due to seismic signal attenuation in irregularly distributed low-velocity gas charged zones (Gorman et al., 2002; Løseth et al., 2002; Arntsen et al., 2007). The upward migration of fluids can affect gas hydrate stability by altering the temperature, salinity of pore fluids, and composition of gas forming hydrates (Judd and Hovland, 2007). The upward fluid flow (and likely upward heat flow) through gas chimneys can significantly shift hydrate stability conditions away from steady state predictions.

It is challenging to estimate the salinity and gas composition variations caused by such a large zone of fluid leakage since we have limited insight into variations in subsurface salinity and gas composition with depth. Nonetheless, it is possible to isolate the effects of temperature by modelling temperature variations in the area as a result of advective heat flow through the gas chimney assuming constant geochemical conditions. In order to understand the role fluid flow might play in shoaling of the BSR we consider an arbitrary 2D line from the 3D P-Cable seismic data (Figure 2) as the geometrical constraint for a 2D steady-state advection-diffusion heat flow model. The horizontal resolution is set to 100 m. The shallowest source rock in the area is Hekkingen formation representing late Jurassic age, which occurs at 1893 mbsl. One of the major source rocks in the area, Snadd Formation representing late Triassic age, is situated at a depth of 2877 mbsl (from well 7219/9-1); however, source rocks across this region extend to depths as great as 3000 mbsl (NPD). Since it is almost impossible to identify the exact depth of

source of fluid flow from the seismic data, we assume a depth of 3000 meters below sea level as the fluid source depth for constant rate advective flow modelling, since this depth should include all possible source rocks present in the area. We use the advection-diffusion equation with constant vertical fluid advection rates to generate a 2D temperature model. We iterate fluid advection rate to determine what flow rates best produce a temperature profile that matches observed BSRs across the region.

We consider a model with constant vertical fluid flow restricted to regions directly below the discontinuous BSR in the 2D seismic line. The width of the zones of fluid flow varies from place to place depending on the width of the BSR. From west to east, the five different zones of vertical fluid flow considered in the model are 400 m, 1100 m, 100 m, 100 m, and 800 m wide respectively (Figure 7b). Keeping all other parameters similar as for the 3D diffusive heat flow model, we generate a 2D steady-state advection-diffusion thermal model for the site assuming vertical fluid flow only (Figure 7a). From this analysis, we find that different vertical flow velocities could exist in the area that might explain BSR depths. To explain the observed anomalous BSR, the fluid flow velocities should be 6, 4.8, 10, 12, and 5.6 mm/year from west to east respectively (Figure 7b). This model provides the simplest explanation for the observed anomalous BSR. It should be noted that these flow rates represent only average, steady-state flow values and that in addition to heat, fluid flow can also cause changes to other parameters controlling hydrate stability such as salinity and gas composition.

6.3 Implications of the fluid flow model

The required flow rates for the model are low and comparable to other advective flow rates in similar gas hydrate and petroleum provinces (Hornbach et al., 2005; Ruppel, 2005; de Beer et al.,

2006). Such moderate submarine fluid flow rates should not be unexpected, and our analysis therefore suggests that fluid flow provides an alternative, simple explanation for the nature of the BSR. Furthermore, our estimated fluid flux is comparable to previous fluid flux estimations from a nearby area by Rajan et al. (2013), who estimated fluid flow velocities of 1.88-2.2 mm/year. Nonetheless it is unlikely that the depth of the BSR is constrained solely by advection, as assumed in our flow model. Fluid advection often transports deeper saline fluids and higher-order hydrocarbons, which, as noted already (Figure 6), affect gas hydrate stability. Without direct measurements of salinity or gas composition in the area, our fluid flow model provides a simple end-member explanation (that assumes no variability in geochemistry or geology) for the BSR observed in the seismic data.

The concept of locally focused fluid conduits with different flow rates at this site, as a viable explanation for the shoaling of the BSR is not necessarily surprising. The detailed internal structure of gas chimneys is poorly understood. A single zone of fluid flow (often denoted as a gas chimney, or pipe) can be, in fact, a network of dendritic conduits (e.g., Løseth et al., 2002; Cartwright et al., 2007; Hornbach et al., 2007; Judd and Hovland, 2007; Connolly et al., 2008). Flow of fluids through different conduits can sometimes manifest itself in seismic data as a single gas chimney where complex vertical and horizontal conduits are below seismic resolution or are masked by the presence of gas (Judd and Hovland, 2007). The velocity of vertical fluid flow could vary depending on the geometry and size of these conduits and the regional temperature and pressure field. The chimneys may also consist of stacked localized amplitude anomalies which result from gas accumulations or cementations (Cartwright et al., 2007). Based on our observation of an irregular and discontinuous BSR over short lateral distances, we suggest variability in fluid flow (and perhaps geochemical) parameters at the meter scale across the site

provide perhaps the simplest explanation for the observed small scale variability in BSR depth. It is important to recognize that the sharpness of these BSR depth irregularities across the section is inconsistent with steady-state diffusive heat flow at the site, implying a dynamic system likely exists. We hypothesize that the observed BSR is perhaps the result of a complex combination of upward fluid flow that likely changes regional geochemistry across the site by upwelling higher-order hydrocarbons and perhaps more saline pore water from depth.

From our modelling, it is evident that fluid flow affects hydrate stability which suggests that the fluid flow system is currently active. Recent observations of gas flares south of the study area by Chand et al. (2012) also suggest an active fluid flow system along the south-north trending fault complexes (Fig. 1). From the predicted fluid flow velocities, we estimate a fluid flux of ~1860 $m^3 year^{-1} km^{-2}$ in to the hydrate stability zone within the area of the 3D seismic data, assuming a continuous flow. Based on the principle of continuity, a similar volume of fluids should reach the shallow subsurface or the ocean from the region considered in this study. However, a myriad of geochemical and biochemical processes, such as formation of authigenic carbonates and utilization of methane by the methanogens and archaea, occur in the near surface which makes it difficult, from the data in hand, to estimate the amount of gas which may enter the shallow sediments or arguably the ocean through the GHSZ.

With more accurate constraints on regional temperature and geochemistry, this method can be used to estimate subsurface fluid flow velocities, and total amount of hydrocarbons entering shallow sediments.

7. Conclusions

Our study demonstrates the role regional geological, geochemical, geophysical conditions play in gas hydrate stability assessments in the SW Barents Sea. Our analysis indicates higher order hydrocarbons exist across this region, implying the deep migration of thermogenic gas at this site. Although changes in heat flow and geochemistry cannot be ruled out, we suggest active fluid flow, focused along specific irregular-shaped conduits in a large chimney structure, provides the simplest explanation for the anomalous BSR we observe in the region. It is highly unlikely given the small scale lateral variations in BSR depth at this site that temperature (or alternatively chemical) regime at this site is in steady state, further supporting the concept that small-scale variations in regional fluid flow exist across the 3D dataset. Fluid flow significantly affects the hydrate stability conditions in the SW Barents Sea mainly by altering the thermal regime in the area. It can also affect the hydrate stability by affecting other parameters such as salinity of pore fluid and compositions of gas forming hydrate by transporting higher-order hydrocarbons from depth. We suggest that the amount of thinning of GHSZ in the SW Barents Sea depends primarily on uncertainties related to fluid flow and regional geochemistry. Ultimately, in situ geochemical and geophysical analysis via drilling and monitoring is necessary to better constrain controls on the GHSZ in the Barents Sea. Nonetheless, our initial modelling provide a first approach at understanding the controls on gas hydrate stability, and how different geological, geochemical, and geophysical parameters can sometimes have a significant impact on hydrate distribution across this geologically complex region.

Acknowledgments

This study was funded by the Research Council of Norway through Leiv Eiriksson mobility program (No.216789/F11). We thank the captain and crew of RV Helmer Hanssen for their assistance in acquiring the 3D P-Cable seismic data. Lundin Petroleum is acknowledged for partly funding for the data acquisition. This research is part of the Centre of Excellence: Arctic Gas hydrate, Environment and Climate (CAGE) funded by the Norwegian Research Council (Grant No. 223259). We thank two anonymous reviewers whose suggestions improved the manuscript. We acknowledge software support by Schlumberger and DECO Geophysical. We are also thankful to DECO Geophysical for processing the P-Cable 3D seismic data. Thanks goes to all members in the Department of Earth Sciences, Southern Methodist University, for making the duration of study in Dallas a pleasant experience.

References

Abdou, M., Carnegie, A., Mathews, S.G., McCarthy, K., O'Keefe, M., Raghuraman, B., Wei, W., Xian, C.G., 2011. Finding Value in Formation Water. Oilfield Review 23, 24-35.

Andreassen, K., Hogstad, K., Berteussen, K.A., 1990. Gas hydrate in the southern Barents Sea, indicated by a shallow seismic anomaly. First Break 8, 235-245.

Andreassen, K., Nilssen, E., Ødegaard, C., 2007. Analysis of shallow gas and fluid migration within the Plio-Pleistocene sedimentary succession of the SW Barents Sea continental margin using 3D seismic data. Geo-Marine Letters 27, 155-171.

Arntsen, B., Wensaas, L., Loseth, H., Hermanrud, C., 2007. Seismic modeling of gas chimneys. Geophysics 72, Sm251-Sm259.

Biastoch, A., Treude, T., Rüpke, L.H., Riebesell, U., Roth, C., Burwicz, E.B., Park, W., Latif, M., Böning, C.W., Madec, G., Wallmann, K., 2011. Rising Arctic Ocean temperatures cause gas hydrate destabilization and ocean acidification. Geophysical Research Letters 38, L08602.

Bredehoeft, J.D., Papadopulos, I.S., 1965. Rates of vertical groundwater movement estimated from the Earth's thermal profile. Water Resources Research 1, 325-328.

Bugge, T., Befring, S., Belderson, R., Eidvin, T., Jansen, E., Kenyon, N., Holtedahl, H., Sejrup, H., 1987. A giant three-stage submarine slide off Norway. Geo-Marine Letters 7, 191-198.

Bugge, T., Elvebakk, G., Fanavoll, S., Mangerud, G., Smelror, M., Weiss, H.M., Gjelberg, J., Kristensen, S.E., Nilsen, K., 2002. Shallow stratigraphic drilling applied in hydrocarbon exploration of the Nordkapp Basin, Barents Sea. Marine and Petroleum Geology 19, 13-37.

Bünz, S., Mienert, J., Berndt, C., 2003. Geological controls on the Storegga gas-hydrate system of the mid-Norwegian continental margin. Earth and Planetary Science Letters 209, 291-307.

Cartwright, J., Huuse, M., Aplin, A., 2007. Seal bypass systems. Aapg Bulletin 91, 1141-1166.

Cavanagh, A.J., Di Primio, R., Scheck-Wenderoth, M., Horsfield, B., 2006. Severity and timing of Cenozoic exhumation in the southwestern Barents Sea. Journal of the Geological Society 163, 761-774.

Chand, S., Mienert, J., Andreassen, K., Knies, J., Plassen, L., Fotland, B., 2008. Gas hydrate stability zone modelling in areas of salt tectonics and pockmarks of the Barents Sea suggests an active hydrocarbon venting system. Marine and Petroleum Geology 25, 625-636.

Chand, S., Thorsnes, T., Rise, L., Brunstad, H., Stoddart, D., Bøe, R., Lågstad, P., Svolsbru, T., 2012. Multiple episodes of fluid flow in the SW Barents Sea (Loppa High) evidenced by gas flares, pockmarks and gas hydrate accumulation. Earth and Planetary Science Letters 331–332, 305-314.

Claypool, G.E., Kaplan, I.R., 1974. The origin and distribution of methane in marine sediments, in: Kaplan, I.R. (Ed.), Natural Gases in Marine Sediments. Plenum Press, New York, pp. 99-139.

Clennell, M.B., Hovland, M., Booth, J.S., Henry, P., Winters, W.J., 1999. Formation of natural gas hydrates in marine sediments: 1. Conceptual model of gas hydrate growth conditioned by host sediment properties. Journal of Geophysical Research: Solid Earth 104, 22985-23003.

Coffin, R., Pohlman, J., Gardner, J., Downer, R., Wood, W., Hamdan, L., Walker, S., Plummer, R., Gettrust, J., Diaz, J., 2007. Methane hydrate exploration on the mid Chilean coast: A geochemical and geophysical survey. Journal of Petroleum Science and Engineering 56, 32-41.

Collett, T.S., Johnson, A.H., Knapp, C.C., Boswell, R., 2009. Natural Gas Hydrates: A Review, in: Collett, T.S., Johnson, A. H., Knapp, C. C., Boswell, R. (Ed.), Natural gas hydrates—Energy resource potential and associated geologic hazards. AAPG Memoir 89, pp. 146-219.

Connolly, D.L., Brouwer, F., Walraven, D., 2008. Detecting fault-related hydrocarbon migration pathways in seismic data: Implications for fault-seal, pressure, and charge prediction. Gulf Coast Association of Geological Societies Transactions 58, 191-203.

de Beer, D., Sauter, E., Niemann, H., Kaul, N., Foucher, J.P., Witte, U., Schlüter, M., Boetius, A., 2006. In situ fluxes and zonation of microbial activity in surface sediments of the Håkon Mosby Mud Volcano. Limnology and Oceanography 51, 1315-1331.

Dickens, G.R., Castillo, M.M., Walker, J.C.G., 1997. A blast of gas in the latest Paleocene: Simulating first-order effects of massive dissociation of oceanic methane hydrate. Geology 25, 259-262.

Dickens, G.R., Quinby-Hunt, M.S., 1997. Methane hydrate stability in pore water: A simple theoretical approach for geophysical applications. Journal of Geophysical Research: Solid Earth 102, 773-783.

Dobrynin, V.M., Korotajev, Y.P., Plyuschev, D.V., 1981. Gas hydrates-A possible energy resource, in: Meyer, R.F., Olson, J. C. (Ed.), Long-term energy resources. Pitman Publishers, Boston, pp. 727-729.

Doré, A.G., 1995. Barents Sea geology, petroleum resources and commercial potential. Arctic 48, 207-221.

Doré, A.G., Jensen, L.N., 1996. The impact of late Cenozoic uplift and erosion on hydrocarbon exploration: offshore Norway and some other uplifted basins. Global and Planetary Change 12, 415-436.

Driscoll, N.W., Weissel, J.K., Goff, J.A., 2000. Potential for large-scale submarine slope failure and tsunami generation along the U.S. mid-Atlantic coast. Geology 28, 407-410.

Duran, E.R., di Primio, R., Anka, Z., Stoddart, D., Horsfield, B., 2013. 3D-basin modelling of the Hammerfest Basin (southwestern Barents Sea): A quantitative assessment of petroleum generation, migration and leakage. Marine and Petroleum Geology 45, 281-303.

Eidvin, T., Jansen, E., Riis, F., 1993. Chronology of Tertiary fan deposits off the western Barents Sea: Implications for the uplift and erosion history of the Barents Shelf. Marine Geology 112, 109-131.

Elverhøi, A., Solheim, A., 1983. The physical environment western Barents Sea, 1:1,500,000, sheet A, surface sediment distribution. Norsk Polar Institutt Rapportserie 179A, 23.

Faleide, J.I., Gudlaugsson, S.T., Jacquart, G., 1984. Evolution of the western Barents Sea. Marine and Petroleum Geology 1, 123-150.

Faleide, J.I., Vågnes, E., Gudlaugsson, S.T., 1993. Late Mesozoic-Cenozoic evolution of the south-western Barents Sea in a regional rift-shear tectonic setting. Marine and Petroleum Geology 10, 186-214.

Gabrielsen, R.H., Færseth, R.B., Jensen, L.N., Kalheim, J.E., Riis, F., 1990. Structural elements of the Norwegian continental shelf Part I: The Barents Sea Region. Norwegian Petroleum Directorate Bulletin 6.

Gorman, A.R., Holbrook, W.S., Hornbach, M.J., Hackwith, K.L., Lizarralde, D., Pecher, I., 2002. Migration of methane gas through the hydrate stability zone in a low-flux hydrate province. Geology 30, 327-330.

Grace, R.D., 1994. Advanced Blowout and Well Control. Gulf Publishing Co., Houston, TX.

Gudlaugsson, S.T., Faleide, J.I., Johansen, S.E., Breivik, A.J., 1998. Late Palaeozoic structural development of the South-western Barents Sea. Marine and Petroleum Geology 15, 73-102.

Heggland, R., 1998. Gas seepage as an indicator of deeper prospective reservoirs. A study based on exploration 3D seismic data. Marine and Petroleum Geology 15, 1-9.

Helgerud, M.B., Dvorkin, J., Nur, A., Sakai, A., Collett, T., 1999. Elastic-wave velocity in marine sediments with gas hydrates: Effective medium modeling. Geophysical Research Letters 26, 2021-2024.

Henriksen, E., Bjørnseth, H.M., Hals, T.K., Heide, T., Kiryukhina, T., Kløvjan, O.S., Larssen, G.B., Ryseth, A.E., Rønning, K., Sollid, K., Stoupakova, A., 2011. Chapter 17 Uplift and erosion of the greater Barents Sea: impact on prospectivity and petroleum systems. Geological Society, London, Memoirs 35, 271-281.

Holbrook, W.S., Hoskins, H., Wood, W.T., Stephen, R.A., Lizarralde, D., 1996. Methane Hydrate and Free Gas on the Blake Ridge from Vertical Seismic Profiling. Science 273, 1840-1843.

Hornbach, M.J., Bangs, N.L., Berndt, C., 2012. Detecting hydrate and fluid flow from bottom simulating reflector depth anomalies. Geology 40, 227-230.

Hornbach, M.J., Holbrook, W., Gorman, A., Hackwith, K., Lizarralde, D., Pecher, I., 2003. Direct seismic detection of methane hydrate on the Blake Ridge. GEOPHYSICS 68, 92-100.

Hornbach, M.J., Ruppel, C., Saffer, D.M., Van Dover, C.L., Holbrook, W.S., 2005. Coupled geophysical constraints on heat flow and fluid flux at a salt diapir. Geophysical Research Letters 32, L24617.

Hornbach, M.J., Ruppel, C., Van Dover, C.L., 2007. Three-dimensional structure of fluid conduits sustaining an active deep marine cold seep. Geophysical Research Letters 34, L05601.

Hovland, M., Gudmestad, O.T., 2001. Potential Influence of Gas Hydrates on Seabed Installations, Natural Gas Hydrates: Occurrence, Distribution, and Detection. American Geophysical Union, pp. 307-315.

Hovland, M., Judd, A.G., 1988. Seabed Pockmarks and Seepages: Impact on Geology, Biology and the Marine Environment. Graham and Trotman Ltd., London.

Hunter, S.J., Goldobin, D.S., Haywood, A.M., Ridgwell, A., Rees, J.G., 2013. Sensitivity of the global submarine hydrate inventory to scenarios of future climate change. Earth and Planetary Science Letters 367, 105-115.

Judd, A., Hovland, M., 2007. Seabed Fluid Flow: The Impact on Geology, Biology and the Marine Environment. Cambridge University Press, Cambridge.

Kjemperud, A., Fjeldskaar, W., 1992. Pleistocene glacial isostasy-implications for petroleum geology, in: Larsen, R.M., Brekke, H., Larsen, B.T., Talleraas, E. (Ed.), Structural and Tectonic Modeling and its Application to Petroleum Geology(NPF Special Publications 1). Elsevier, Amsterdam, pp. 187-195.

Knies, J., Damm, E., Gutt, J., Mann, U., Pinturier, L., 2004. Near-surface hydrocarbon anomalies in shelf sediments off Spitsbergen: Evidences for past seepages. Geochemistry, Geophysics, Geosystems 5, Q06003.

Knies, J., Matthiessen, J., Vogt, C., Laberg, J.S., Hjelstuen, B.O., Smelror, M., Larsen, E., Andreassen, K., Eidvin, T., Vorren, T.O., 2009. The Plio-Pleistocene glaciation of the Barents Sea–Svalbard region: a new model based on revised chronostratigraphy. Quaternary Science Reviews 28, 812-829.

Kvenvolden, K.A., 1988. Methane hydrate — A major reservoir of carbon in the shallow geosphere? Chemical Geology 71, 41-51.

Kvenvolden, K.A., 1998. A primer on the geological occurrence of gas hydrate. Geological Society, London, Special Publications 137, 9-30.

Kvenvolden, K.A., Lorenson, T.D., 2001. The Global Occurrence of Natural Gas Hydrate, Natural Gas Hydrates: Occurrence, Distribution, and Detection. American Geophysical Union, pp. 3-18.

Laberg, J.S., Andreassen, K., 1996. Gas hydrate and free gas indications within the Cenozoic succession of the Bjornoya Basin, western Barents Sea. Marine and Petroleum Geology 13, 921-940.

Laberg, J.S., Andreassen, K., Knutsen, S.M., 1998. Inferred gas hydrate on the Barents Sea shelf — a model for its formation and a volume estimate. Geo-Marine Letters 18, 26-33.

Larsen, R.M., Fjæran, T., Skarpnes, O., 1993. Hydrocarbon potential of the Norwegian Barents Sea based on recent well results, in: Vorren, T.O., Bergsager, E., Dahl-Stamnes, Ø.A., Holter, E., Johansen, B., Lie, E., Lund, T. (Ed.), Arctic geology and petroleum potential. Elsevier, Amsterdam, pp. 321-331.

Løberg, R., Bjorøy, M., 1990. Surface geochemical survey of Bjørnøya west. Geolab Nor A/S, Unpublished report, p. 400.

Løseth, H., Wensaas, L., Arntsen, B., 2002. Gas chimneys – indication of fractured cap rocks, AAPG Hedberg Conference, Vancouver, BC, Canada.

Løvø, V., Elverhøi, A., Antonsen, P., Solheim, A., Butenko, G., Gregersen, O., Liestøl, O., 1990. Submarine permafrost and gas hydrates in the northern Barents Sea. Norsk Polar Institutt Rapportserie 56, 171.

MacDonald, G., 1990. Role of methane clathrates in past and future climates. Climatic Change 16, 247-281.

McConnell, D.R., Zhang, Z., Boswell, R., 2012. Review of progress in evaluating gas hydrate drilling hazards. Marine and Petroleum Geology 34, 209-223.

McIver, R.D., 1982. Role of Naturally Occurring Gas Hydrates in Sediment Transport. The American Association of Petroleum Geologists Bulletin 66, 789-792.

Mienert, J., Posewang, J., Lukas, D., 2001. Changes in the Hydrate Stability Zone on the Norwegian Margin and their Consequence for Methane and Carbon Releases Into the Oceanosphere, in: Schäfer, P., Ritzrau, W., Schlüter, M., Thiede, J. (Eds.), The Northern North Atlantic. Springer Berlin Heidelberg, pp. 259-280.

Milkov, A.V., 2000. Worldwide distribution of submarine mud volcanoes and associated gas hydrates. Marine Geology 167, 29-42.

Milkov, A.V., Claypool, G.E., Lee, Y.-J., Xu, W., Dickens, G.R., Borowski, W.S., Party, O.L.S., 2003. In situ methane concentrations at Hydrate Ridge, offshore Oregon: New constraints on the global gas hydrate inventory from an active margin. Geology 31, 833-836.

Nisbet, E.G., 1989. Some northern sources of atmospheric methane: production, history, and future implications. Canadian Journal of Earth Sciences 26, 1603-1611.

Nisbet, E.G., 2002. Have sudden large releases of methane from geological reservoirs occurred since the Last Glacial Maximum, and could such releases occur again? Philosophical Transactions of the Royal Society of London. Series A: Mathematical, Physical and Engineering Sciences 360, 581-607.

NODC, 2013. World Ocean Database (http://www.nodc.noaa.gov/General/temperature.html).

NPD, Factpages. Nowegian Petroleum Directorate (http://factpages.npd.no/factpages/).

Nyland, B., Jensen, L.N., Skagen, J., Skarpnes, O., Vorren, T.O., 1992. Tertiary uplift and erosion in the Barents Sea: Magnitude, timing and consequences, in: Larsen, R.M., Brekke, H., Larsen, B.T., Talleraas, E. (Ed.), Structural and Tectonic Modeling and its Application to Petroleum Geology(NPF Special Publications 1). Elsevier, Amsterdam, pp. 153-162.

Nøttvedt, A., Berglund, L.T., Rasmussen, E., Steel, R.J., 1988. Some aspects of Tertiary tectonics and sedimentation along the western Barents Shelf. Geological Society, London, Special Publications 39, 421-425.

Ostanin, I., Anka, Z., di Primio, R., Bernal, A., 2012. Identification of a large Upper Cretaceous polygonal fault network in the Hammerfest basin: Implications on the reactivation of regional faulting and gas leakage dynamics, SW Barents Sea. Marine Geology 332–334, 109-125.

Perez-Garcia, C., Feseker, T., Mienert, J., Berndt, C., 2009. The Håkon Mosby mud volcano: 330 000 years of focused fluid flow activity at the SW Barents Sea slope. Marine Geology 262, 105-115.

Peters, K.E., Nelson, P.H., 2009. Criteria to Determine Borehole Formation Temperatures for Calibration of Basin and Petroleum System Models, AAPG Annual Convention and Exhibition, Denver, Colorado, USA.

Pham, T.H.V., Maast, T.E., Hellevang, H., Aagaard, P., 2011. Numerical modeling including hysteresis properties for CO2 storage in Tubåen formation, Snøhvit field, Barents Sea. Energy Procedia 4, 3746-3753.

Phrampus, B.J., Hornbach, M.J., 2012. Recent changes to the Gulf Stream causing widespread gas hydrate destabilization. Nature 490, 527-530.

Planke, S., Eriksen, F.N., Berndt, C., Mienert, J., Masson, D., 2009. Spotlight on Technology: P-Cable High-Resolution Seismic. Oceanography 22, 85.

Prince, P.K., 1990. Current drilling practice and the occurrence of shallow gas, in: Ardus, D.A., Green, C. D. (Ed.), Safety in Offshore Drilling: the Role of Shallow Gas Surveys. Kluwer Academic Publishers, Dordrecht, pp. 3-25.

Rajan, A., Bünz, S., Mienert, J., Smith, A.J., 2013. Gas hydrate systems in petroleum provinces of the SW-Barents Sea. Marine and Petroleum Geology 46, 92-106.

Riis, F., Fjeldskaar, W., 1992. On the magnitude of the late Tertiary and Quarternary erosion and its significance for the uplift of Scnadinavia and the Barents Sea, in: Larsen, R.M., Brekke, H., Larsen, B.T., Talleraas, E. (Ed.), Structural and Tectonic Modelling and its Application to Petroleum Geology. Norsk Petroleum Society Special Publication 1. Elsevier, Amsterdam, pp. 163–185.

Ruppel, C., 2005. Heat and salt inhibition of gas hydrate formation in the northern Gulf of Mexico. Geophysical Research Letters 32, L04605.

Ruppel, C., Boswell, R., Jones, E., 2008. Scientific results from Gulf of Mexico Gas Hydrates Joint Industry Project Leg 1 drilling: Introduction and overview. Marine and Petroleum Geology 25, 819-829.

Shipley, T.H., Houston, M.H., Buffler, R.T., Shaub, F.J., McMillen, K.J., Ladd, J.W., Worze, J.L., 1979. Seismic Evidence for Widespread Possible Gas Hydrate Horizons on Continental Slopes and Rises. AAPG Bulletin 63, 2204-2213.

Sloan, E.D., Koh, C.A., 2008. Clathrate Hydrates of Natural Gases, Third Edition. CRC Press, Boca Raton, FL.

Svendsen, J.I., Alexanderson, H., Astakhov, V.I., Demidov, I., Dowdeswell, J.A., Funder, S., Gataullin, V., Henriksen, M., Hjort, C., Houmark-Nielsen, M., Hubberten, H.W., Ingólfsson, Ó., Jakobsson, M., Kjær, K.H., Larsen, E., Lokrantz, H., Lunkka, J.P., Lysså, A., Mangerud, J., Matiouchkov, A., Murray, A., Möller, P., Niessen, F., Nikolskaya, O., Polyak, L., Saarnisto, M., Siegert, C., Siegert, M.J., Spielhagen, R.F., Stein, R., 2004. Late Quaternary ice sheet history of northern Eurasia. Quaternary Science Reviews 23, 1229-1271.

Talleraas, E., 1979. The Hammerfest Basin-an aulacogen? Proceedings, Norwegian Sea Symposium, Norwegian Petroleum Society 18, 1-13.

Taylor, M.H., Dillon, W.P., Pecher, I.A., 2000. Trapping and migration of methane associated with the gas hydrate stability zone at the Blake Ridge Diapir: new insights from seismic data. Marine Geology 164, 79-89.

Ussler, W., Paull, C.K., 2001. Ion Exclusion Associated with Marine Gas Hydrate Deposits, Natural Gas Hydrates: Occurrence, Distribution, and Detection. American Geophysical Union, pp. 41-51.

Vadakkepuliyambatta, S., Bünz, S., Mienert, J., Chand, S., 2013. Distribution of subsurface fluid-flow systems in the SW Barents Sea. Marine and Petroleum Geology 43, 208-221.

Vorren, T.O., Hald, M., Lebesbye, E., 1988. Late Cenozoic environments in the Barents Sea. Paleoceanography 3, 601-612.

Vorren, T.O., Richardsen, G., Knutsen, S.M., Henriksen, E., 1991. Cenozoic erosion and sedimentation in the western Barents Sea. Marine and Petroleum Geology 8, 317-340.

Waite, W.F., Helgerud, M.B., Nur, A., Pinkston, J.C., Stern, L.A., Kirby, S.H., Durham, W.B., 2000. Laboratory Measurements of Compressional and Shear Wave Speeds through Methane Hydrate. Annals of the New York Academy of Sciences 912, 1003-1010.

Warren, J.K., 2006. Evaporites: Sediments, Resources and Hydrocarbons. Springer, Berlin, Germany.

Woodside, J., Ivanov, M., 2002. Is there a shallow BSR in the eastern Mediterranean?, Gas in Marine Sediments, Seventh International Conference. Nafta Press, Baku, Azerbaijan, pp. 189-191.

Yakushev, V., Collett, T., 1992. Gas hydrates in Arctic regions-risks to drilling and production, International Offshore and Polar Engineering Conference, Golden, CO, pp. 669-673.

Figure Captions

Figure 1. Location and bathymetry of the study area along with locations of the 3D and 2D seismic data, location of gas chimneys in the area (Vadakkepuliyambatta et al., 2013) (white shaded), major structural elements (NPD), and bottom water temperature contours (NODC, 2013)

Figure 2. a) P-Cable 3D seismic data along with seafloor time surface. The seismic data shows high-amplitude, reverse polarity reflector, which is interpreted as a BSR, and chaotic seismic reflections below. Zones of vertical fluid flow are marked. Seafloor time surface shows high concentration of crisscrossing glacial plough marks as wide as 200m b) Zoomed in view of the BSR from the P-Cable data (for location see figure 3a) which clearly shows the sharp dipping reflections. Seismic trace (yellow) shows the anomalously high amplitude of the BSR. c) Another part (for location see figure 3a) of the P-Cable seismic data is zoomed to highlight the cross-cutting nature of the reflection.

Figure 3. a) P-Cable 3D seismic cube showing high-amplitudes (in blue) from an RMS amplitude map. It highlights the distribution of discontinuous BSRs exhibiting various shapes in the study area. b) 2D seismic profile (for location see figure 3a) show much wider occurrence of the BSR. It also shows the dipping edges of discontinuous BSRs. A seismic trace (yellow) shows the polarity reversal at the BSR with respect to the seafloor.

Figure 4. a) Plot showing the geothermal gradient, measured and Horner-corrected bottom-hole temperatures. b) Checkshot data from well 7219/9-1 illustrating the relation between two-way time (TWT) depth and average seismic velocity. c) Temperature and seismic velocity of the water column from CTD data (location in Fig. 1).

Figure 5. a) 2D section from the 3D thermal model generated using diffusive heat flow modelling, showing a generally uniform distribution of heat resulting from a relatively flat seafloor. b) Seismic profile showing predicted BSR in comparison with the observed BSR. The maximum anomaly between observed and predicted BSR is estimated to be approximately 55 m.

The transparent grey region show estimated uncertainty in model predictions. c) Thickness map between observed BSR and predicted BSR. It varies from 8 m to 55 m.

Figure 6. Uncertainties associated with the model. The variation of each parameter in the SW Barents Sea is considered and its effect on the BSR depth.

Figure 7. a) Thermal profile generated by 2D advective-diffusive heat flow model show slight upward shift in the thermal profile in areas where upward fluid flow exists. b) Seismic profile showing BSR modelled using the advective-diffusive heat flow model. Also shown are the vertical fluid flow zones considered in the model and estimated fluid flow velocities through them. This model provides the best fit between modelled and observed BSRs.

Figure 1

Click here to download high resolution image

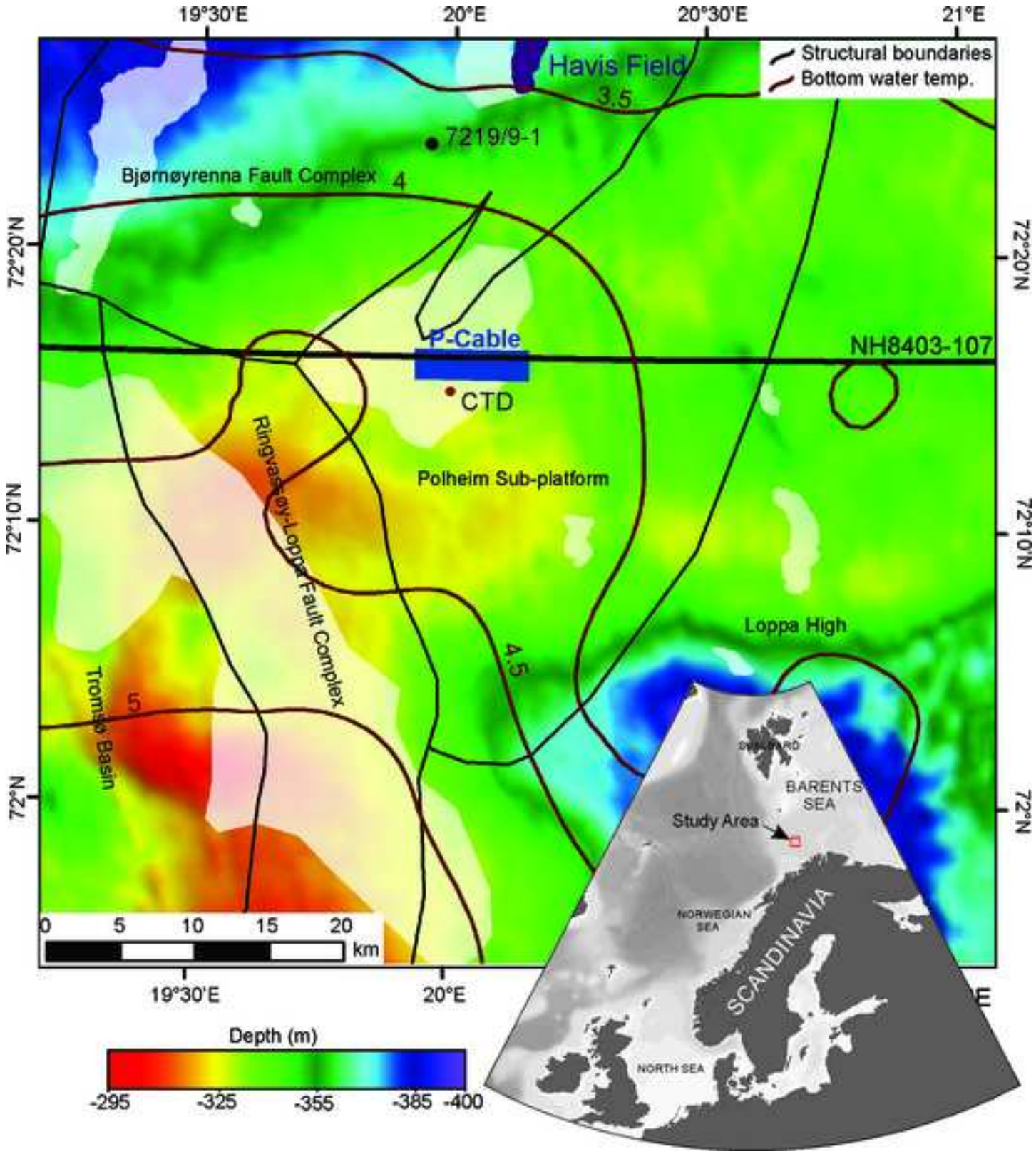

Figure 2

Click here to download high resolution image

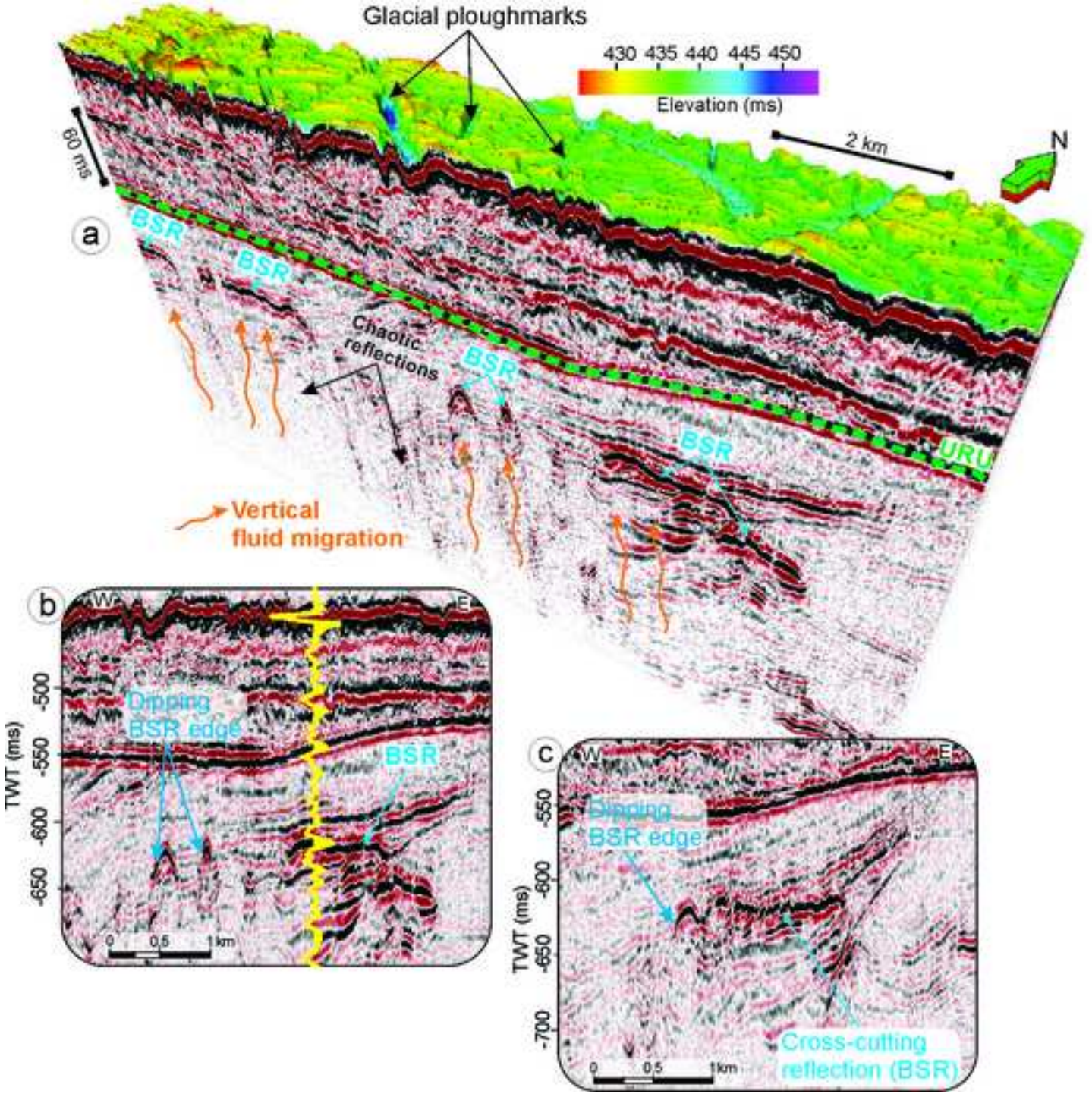

Figure 3

Click here to download high resolution image

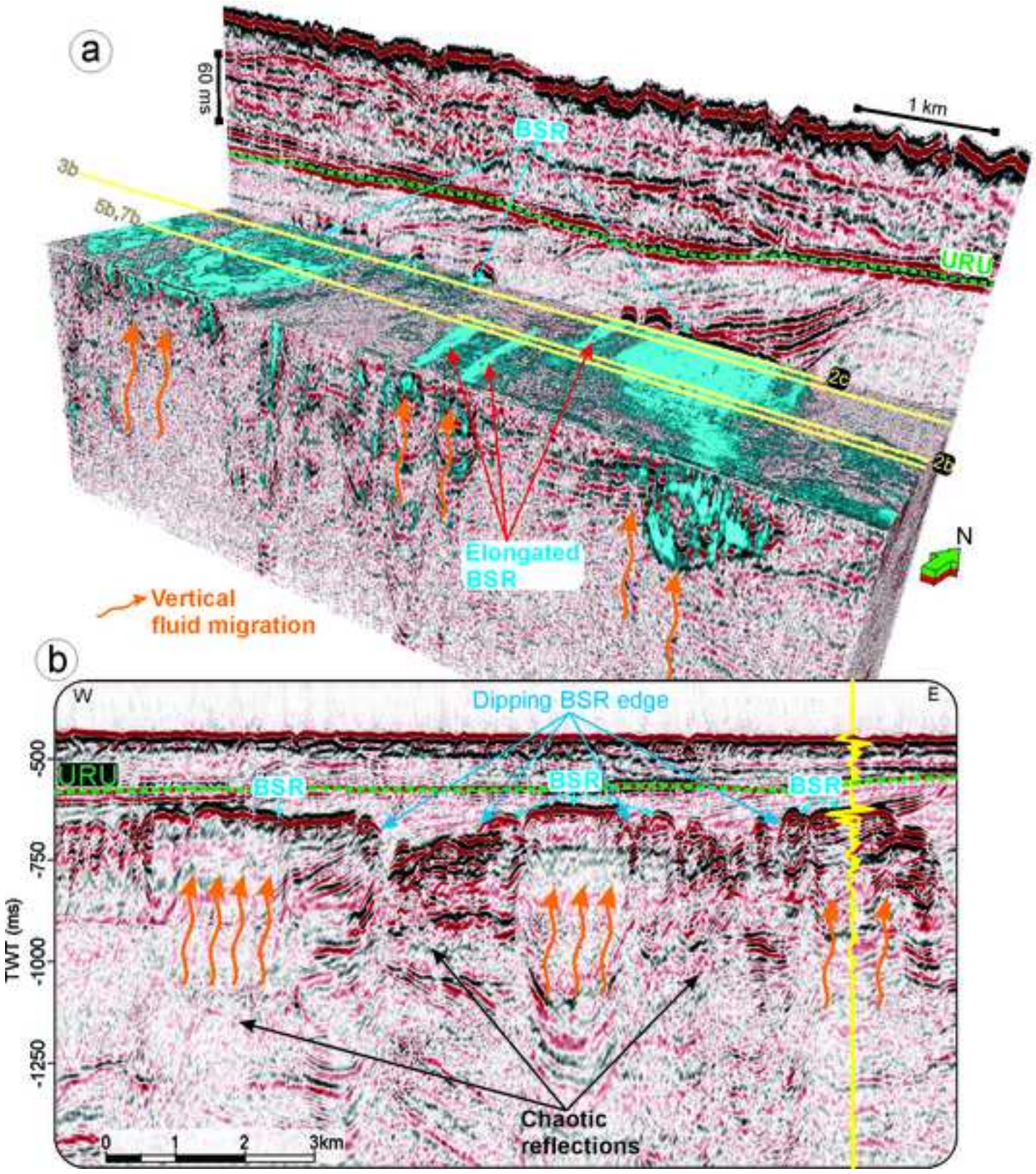

Figure 4

Click here to download high resolution image

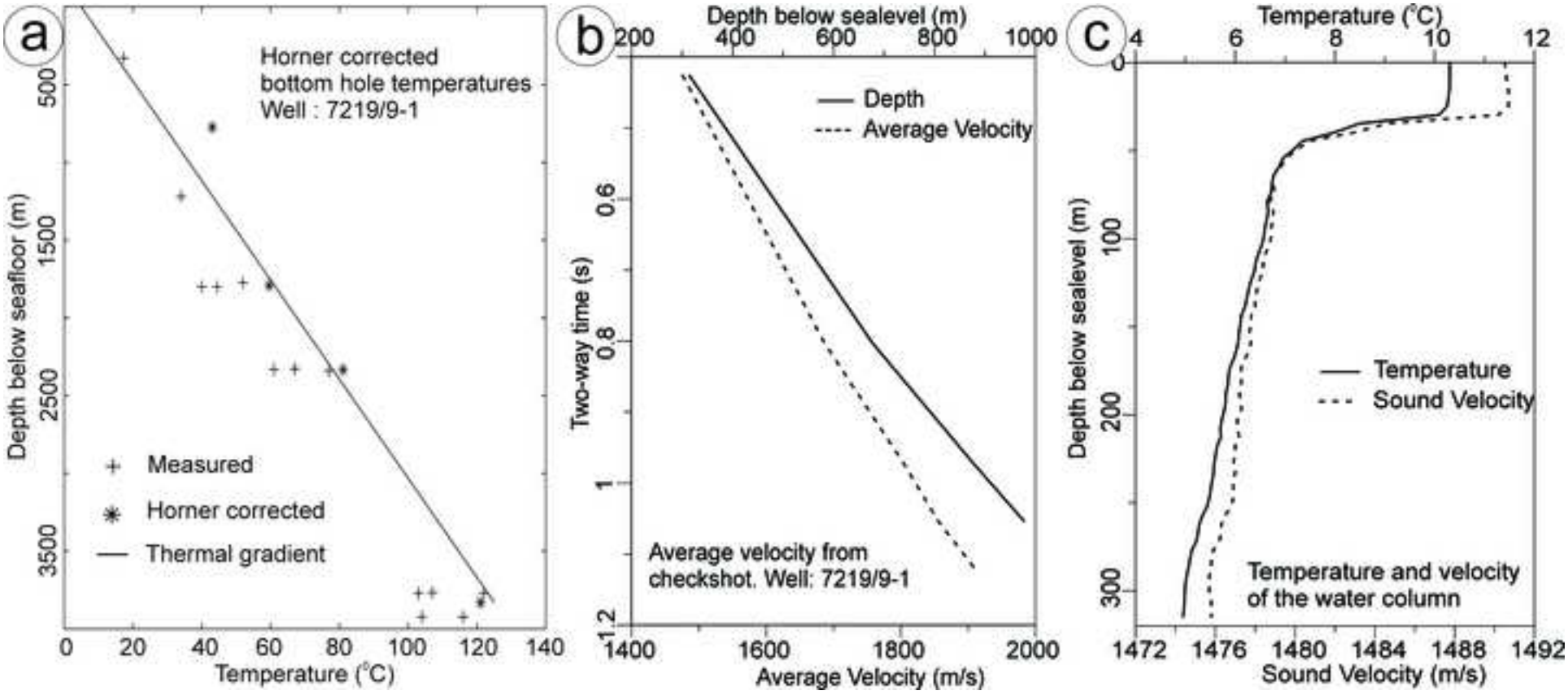

Figure 5

Click here to download high resolution image

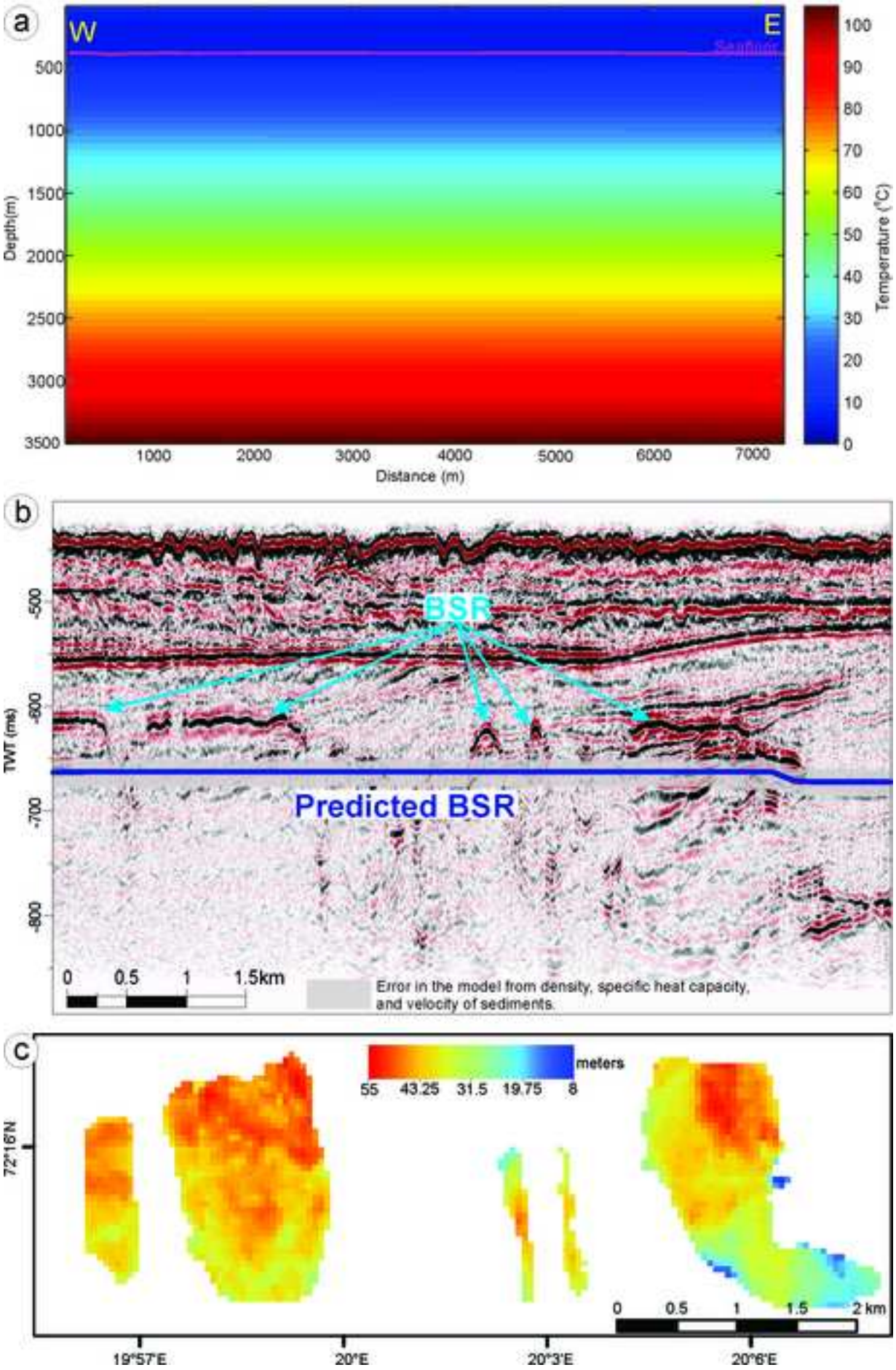

Figure 6

Click here to download high resolution image

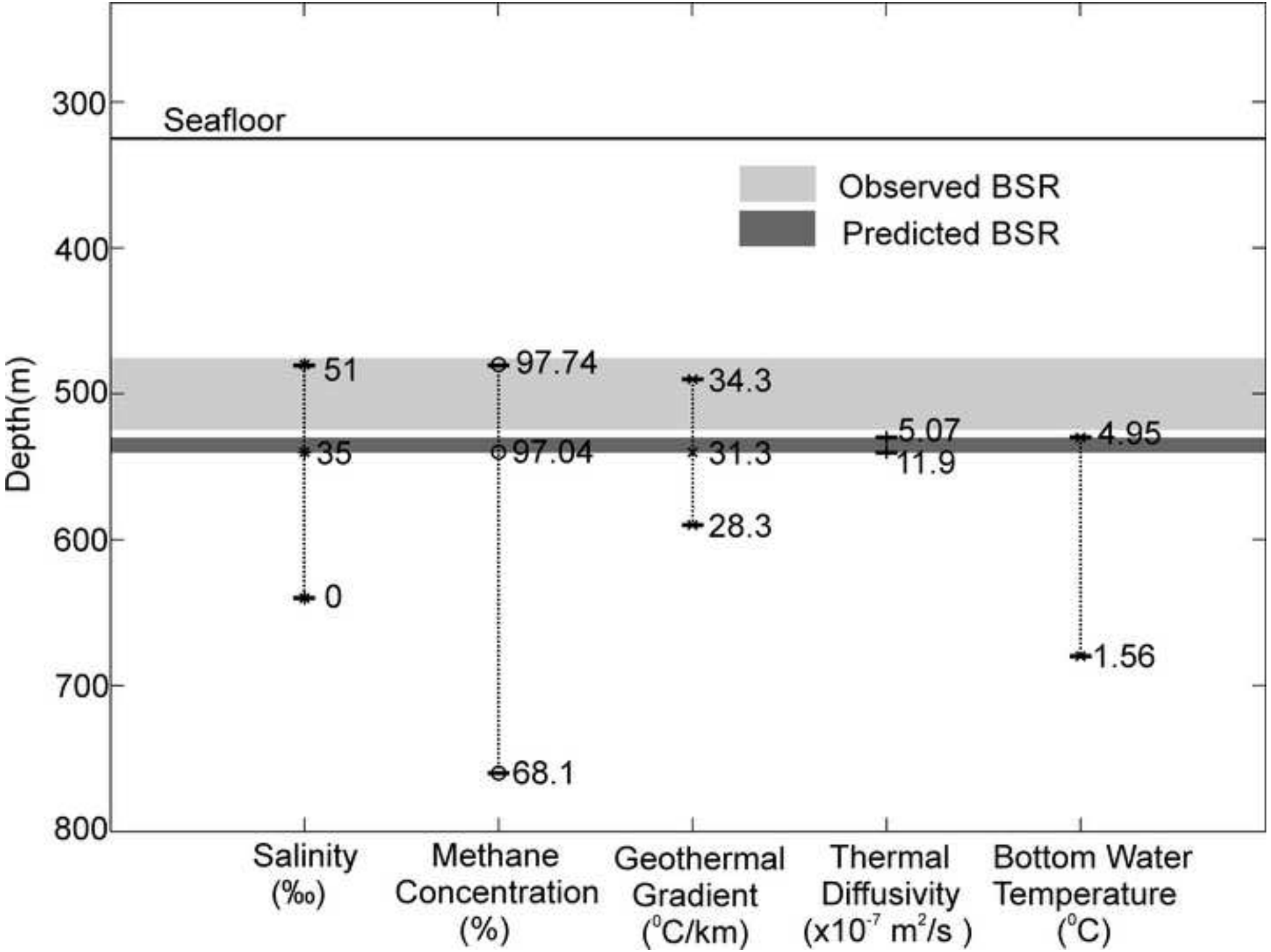

Figure 7

Click here to download high resolution image